sustainability

MDPI

Type of the Paper (Article, Review, Communication, etc.)

Experimental study on pore pressure variation and erosion stability of sandy slope model under MICP

Mingjuan Huang[1]: Jinning Hu[2] and Yunpeng Hei [2] ,Zikun Xu[1],Jinchen Su[1], Youliang Zhang [2,*]

[1] Hainan Provincial Water Conservancy and Hydropower Group CO.,
[2] School of Civil Engineering and Architecture, Hainan University, Haikou 570228, China;
zhangyouliang@hainanu.edu.cn(Y.L.);29930576@qq.com(M.J.) ;1146142979@qq.com(Y.P.);
35525986@qq.com(Z.K.);996653282@qq.com(J.C.);
* Correspondence: zhangyouliang@hainanu.edu.cn

Abstract: With the development of a free trade port on Hainan Island, the construction of tourist roads around the island is currently underway. However, the weather conditions on Hainan Island, which include strong typhoons and rainstorms, pose challenges for the construction of highway-cutting slopes on the coastal weak sandy terraces. These slopes are susceptible to sand loss and erosion from rainfall. To address this issue, MICP green spray irrigation solidification technology is used to strengthen the sandy cutting, and pore water pressure monitoring is carried out on the slope model during MICP solidification and rainfall scour. Combined with the model pore water pressure and flow slip failure pattern, a dynamic analysis was conducted. The results show that MICP sprinkler irrigation technology can solidify the surface of the slope model in a short time, and after three sets of rotation reinforcement, the model achieved a cementation depth of 4cm, with a well-reinforced surface and closely connected sand samples. Under the erosion effect of simulated rainfall intensity, the sand loss of the slope is weakened, without damage to sand binding damage and the integrity is enhanced. The cementation between sand grains facilitated the conversion of most rainfall into runoff. However, despite these efforts, the slope eventually slid after 150 seconds. During the sliding process, the leading edge of the slope model lost sand and became unloaded, and the failure mode was graded creep slip failure. Finally, the slope was divided into several blocks due to the continuous expansion of cracks following the slope failure. The erosion stability of the sandy slope under heavy rains is optimized and the sand loss is prevented effectively. This study proposes a new method of MICP remediation techniques that serve as a new test basis for the practical application of MICP technology in engineering projects.

Keywords: MICP; Sandy slope; Pore water pressure; Fluid-slip pattern

Citation: To be added by editorial staff during production.

Academic Editor: Firstname Lastname

Received: date
Revised: date
Accepted: date
Published: date

Copyright: © 2023 by the authors. Submitted for possible open access publication under the terms and conditions of the Creative Commons Attribution (CC BY) license (https://creativecommons.org/licenses/by/4.0/).

1. Introduction

In most projects located in tropical areas, many soil slopes are distributed under natural conditions or for engineering purposes. Engineering measures can be used to strengthen soil slope, among which the use of microbial grouting to improve to enhance soil slope stability holds significant engineering application value. At the same time, abundant rain and typhoon often lead to the unsaturated state of slope soil, and continuous heavy rain causes rainwater to infiltrate into slope soil. This results in an increased saturation of slope soil and reduced matric suction of unsaturated soil. Consequently, there is a substantial reduction in the shear strength of slope soil and a surge in the possibility of landslide disasters. Therefore, it is of great theoretical and engineering value to study the stability of slope reinforced by microbial grouting under the condition of rainfall infiltration.

The technology of Microbially induced carbonate precipitation (MICP) utilizes the metabolic reactions of the Bacillus bacteria and the nutrients present in the culture envi-

ronment to promote a series of chemical reactions. This bacterium is abundant in the soil, well adapted to the environment and decomposes man-made urea at an extremely fast rate. Nutrients are absorbed through the nitrification and decomposition reaction and converted into products mainly composed of carbonate. These products gather free ions to form large complex groups, which exhibit a strong cementation effect and adsorb the generated calcium carbonate crystals around the sclerotium. At the same time, the continuous production of CO_3^{2-} ions from decomposition is transported to the surface of bacteria and combined with Ca^{2+} ions adsorbed on the outer surface to precipitate calcium carbonate. Through these calcium carbonate "Bridges", the surrounding loose particles can be condensed into a structurally robust whole, which can fill the pores of the sand body [1-2]. The main biochemical equation of calcium carbonate precipitation induced by microorganisms is as follows [3]:

$$Cell+Ca^{2+} \rightarrow Cell\text{-}Ca^{2+} \quad (1)$$

$$NH_2\text{-}CO\text{-}NH_2+2H_2O \rightarrow 2NH_4^{+}+CO_3^{2-}+Cell+Ca^{2+} \quad (2)$$

$$CO_3^{2-}+Cell\text{-}Ca^{2+} \rightarrow Cell\text{-}CaCO_3\downarrow \quad (3)$$

Based on this reaction mechanism, many scholars at home and abroad have conducted in-depth studies on grouting materials, methods, liquefaction and other aspects [3]. Shao Guanghui et al. [4] found that bacterial biomass was the fundamental factor affecting microbial solidification, with a linear decrease of the bacterial content along the reinforcement channel and a gradual decline in activity. Li Xian [5] et al., based on soil permeability characteristics and on the premise of the compatibility of microbial survival, conducted tests on the applicability of MICP sand for several soils. They concluded that the reaction environment of MICP hydrolysis and induced formation of calcium carbonate is liquid, making it more suitable for sand soil. Xu Pengxu [6] et al. performed single-channel reinforcement with a peristaltic pump on sand samples of different particle sizes. They concluded that if the pores of sand samples were too small, the upper part of sand samples would be prone to blockage, leading to an uneven reinforcement effect. On the other hand, if the particle size was too large, the cementation effect would not be ideal, because the liquid could not easily remain, resulting in a smaller microbial contact surface. In another study, Whiffin[7] performed a long sand column test lasting 5 days and set the consolidation drainage shear test under 50 kPa confining pressure. After the test, the strength of the sand column reached 200kPa~570kPa. Ma Ruinan [8] et al. used the mixing method to explore the permeability characteristics of calcareous sand. They found that MICP technology can reduce the permeability coefficient of calcareous sand by 1 to 2 orders of magnitude, improve the adhesion of calcareous sand, and prevent the sand skeleton from being easily eroded by seepage. Liu et al. [9] conducted a relevant experimental study on MICP-reinforced calcareous sand. Their results showed that an increase in calcium carbonate content would not affect the peak internal friction angle of the reinforced soil, but increased the cohesion of the soil.

In view of the mechanical properties of MICP-reinforced sand, Feng et al. [11] studied the influences of different confining pressures and cementation degrees on the mechanical properties of quartz sand through triaxial drainage tests. The results demonstrate that the strength, dilatancy and initial elastic modulus of MICP-reinforced sand are directly proportional to the degree of cementation, and the degree of cementation is found to be closely linked to the bonding force. Yiman Bing et al. [12-13] conducted experiments that measured the shear strength, compressibility and other properties of the MICP-reinforced coastal soft soil. The outcomes indicated that MICP technology could

improve the compression characteristics of the soft soil and improve the shear strength of the reshaped soil. Tang Yang proposed the parameter-sensitive sequence and combination scheme for MICP-reinforced soft soil. Yin Liyang et al. [14-15] conducted research to verify the correlation between soil strength and calcium carbonate generation. They found that the content of calcium carbonate represented the overall level of cementation in the soil.

At present, there is limited research on the applicability of MICP-reinforced slopes under rainfall erosion and infiltration conditions. Rainfall infiltration is a major factor for an increase in the water content of slopes and a decrease in the shear strength of soil on slopes, leading to a decline in slope under stability. As water content rises, the anti-sliding force of the slope decreases. Hu Qizhi et al. [16] used MIDAS/GTS software to analyze and calculate the stability of slopes under fluid-structure coupling under the influence of matress suction effects. They proved that microbial reinforcement mitigates the influence of rainfall infiltration on slopes, reduces the negative pressure area of pore water pressure on the slope and improves the stability of the slope under rainfall conditions. Wang Zhaoyang [17] et al. conducted tests where they changed the water level in the model to reveal the correlation between the changes in groundwater level and the pore water in the soil. They observed that the negative pressure of unsaturated soil increases under the action of rainfall and loading, indicating a relationship between the change of pore water pressure and the water content in the soil. Zeng Qiang [18] conducted a comparative analysis of influencing factors such as pore water pressure, volume water content and shear stress of slope under rainfall conditions. Their findings revealed that with increasing rainfall intensity under constant rainfall duration, the changes in shear strain and displacement of slope surface also increase, and the shear strain of slope soil gradually moves inward and backwards, especially at the foot of the slope where stress concentration is obvious. The increase in shear strain will cause the slope instability.

At present, both domestic and international scholars have conducted in-depth research on MICP-reinforced sand bodies, but there is still a lack of research on coastal fine sand, and the study on solidified marine fine sand is limited. In the existing research results, most of the reinforcement methods adopted in the study include single-channel grouting reinforcement, mixing reinforcement and direct irrigation, and there is little research on sprinkler irrigation reinforcement. This method has the advantage of maximizing the contact between bacterial liquid and air promoting the vaporization of the bacterial liquid and increasing the contact area with sand samples. As a result, it induces the generation of a large number of calcium carbonate crystals and improves the reinforcement effect. There are few studies on the sandy slope reinforced by MICP under the action of rainfall. Therefore, it is necessary to further analyze the related factors that affect the reinforcement effect of the water solubility of calcium carbonate generated after reinforcement when the water content is high. Additionally, it is essential to study particle connectivity under high pore water pressure conditions.

Based on microbial grouting to strengthen the slope, this study applied the microbial mortar generated by microbial grouting for the slope reinforcement. Grouting tests were conducted to obtain valuable data on microbial grouting. The comparison was made between pore water pressure parameters and flow slip morphology of soil samples after grouting. Based on these comparisons, it is comprehensively evaluated that the microbial mortar slope after grouting exhibited improved water stability and erosion resistance under the action of heavy rainfall, which improves the safety factor of the slope.

2. Test materials and devices

2.1. Test sandn

The medium fine sand used in the test was extracted from the actual engineering site with standard roundness. Adjacent to the site were new road cuts, containing pical beach terrace sand. The engineering environment is shown in the figure.



(**a**) (**b**)

Figure 1. Engineering field.

Indoor soil tests were conducted on the sampled soil according to the Geotechnical Test Regulations. The dry density of the sand sample was measured at 1.64g/cm³, as shown in Table.1. The sand exhibited minimal cohesion, and the basic physical parameters and particle gradation curves are illustrated in FIG 3.



Fig 2. In-situ sand sample

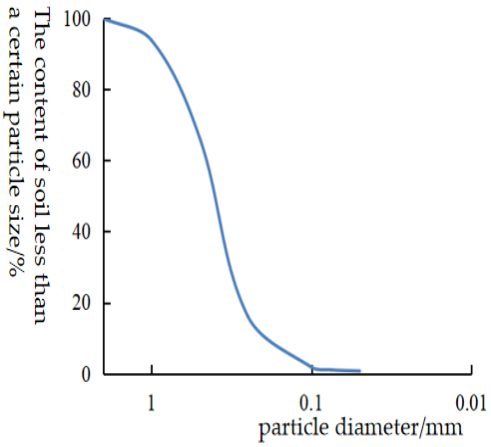


Fig 3. Grain composition

Table 1. Sand property.

Dry density(ρ)	Specific gravity(G_s)	Moisture content(%)	Poriness	Cohesion(C)	Internal friction angle(φ)
1.64	2.66	15	0.29	0	34

2.2. Microbial material

The microbial solidified strain used in the laboratory belongs to Bacillus and was purchased from Shanghai Preservation Biotechnology Center under the name ATCC11859. It was activated by freeze-dried powder in the biological laboratory into 500mL liquid bacterial solution with OD600=2.0.



Figure 4. Bacterial stock solution.

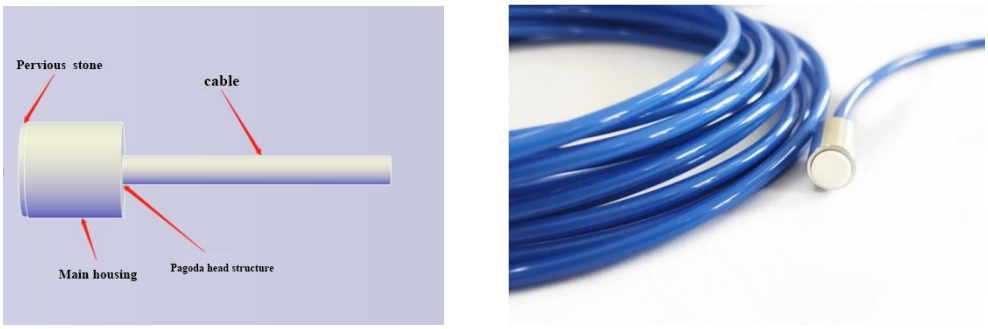
Table 2. Main components and contents of liquid medium.

Composition	Distilled water	Bacteriological peptone	Glucose	NaCl
Content	1L	20g/L	20g/L	10g/L

100mL of the prepared liquid medium subjected to sterilization by steam at 120℃. Next, NaOH solution was added to adjust the pH value of the medium to 9.2. Subsequently, 20mL1mol/L urea solution was added, and the cooled bacterial solution was inoculated into the medium at an 8% inoculum volume with a pipette gun. Following inoculation, the strains were incubated in a shaking bed at 30℃ with a shaking frequency of 180r/m. After an incubation period of 27h, the OD600 of the bacterial solution ranged from 0.6 to 0.8, as measured by a spectrophotometer while the urease activity reached a range of 400~600μs/cm, as measured by a conductivity meter.

2.3. Testing apparatus

The test utilized the DH3818Y Static stress-strain data acquisition instrument manufactured by Donghua Company, which comprises 16 channels. The pore water pressure sensor used in the experiment was procured from Harbin Dayigangzhen Technology Co., LTD. The sensor, named SDYH-DSPP-1 integrated miniature osmotic pressure sensor, is designed to measure negative pressure with a range of -50~50kPa (piezoresissive type). It conforms to international standard sensors to monitor and measure the dynamic pore pressure changes in the slope rainfall model, as illustrated in FIG.5. The measured signal of the sensor represents the change of pore water pressure by the voltage change rate, and the calibration coefficient is shown in Table 3.



(**a**) (**b**)

Figure 5. Stress-strain data acquisition instrument is a figure: (**a**) Sensor constructionl; (**b**) Picture of real products.

Table 3. Sensor calibration coefficient.

Sensor	Calibration coefficient

1	3298.62kPa/V
2	3316.59kPa/V
3	3501.72kPa/V
4	3207.78kPa/V
5	3279.31kPa/V

The overall dimensions of the model box are shown in Figure 6, with length, width and height of 500mm, 500mm and 200mm respectively. The box is constructed with three sides made of 10mm thick toughened glass, while the bottom is a 5mm thick steel plate. The model box is reinforced with steel plate columns at its four corners. Six circular drainage holes with a diameter of 4mm are distributed at the bottom of the model, forming a 3×2 symmetrical pattern. The drainage holes should meet the basic requirements for proper drainage, and the liquid at the bottom should not be redundantly precipitated, which will affect the experimental results.

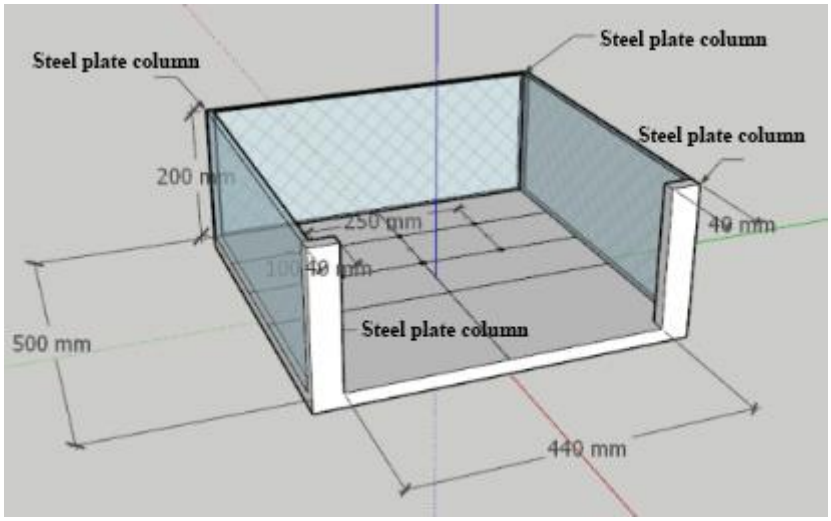
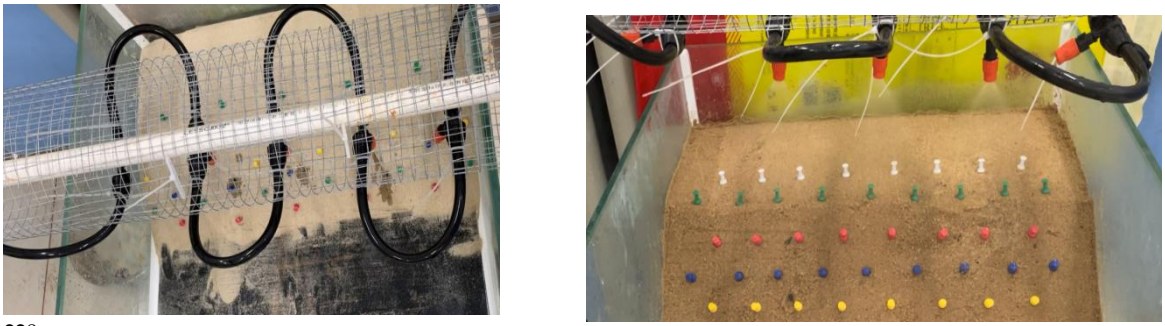


Figure 6. Model box size schematic.

Based on the actual MICP curing condition, a specialized injection device was designed, which consisted of a pump, five nozzles, a timer and multiple hoses. The solution was vaporized by surface spray method to increase the reaction surface area of bacterial solution adhesion. The pump used in the injection device has a maximum power of 45W, and it can deliver a flow parameter of 4L/min. The hoses are fixed after winding the axis for four turns, and all five sprinkler heads are situated on the same plane. The device can move left and right along the axis and rotate 360° to cover the required spraying surface area for the experiment. According to a certain number of spraying times and spraying volume, the fixed liquid, bacterial liquid and cementing liquid are sprayed vertically onto the slope, and the spraying device is positioned 300mm away from the top of the slope. Unlike the single-channel reinforcement method, the reinforcement time can be reduced to less than 1 minute, which greatly improves the reinforcement efficiency.



(**a**) (**b**)

Fig.7 Sprinkler irrigation equipment

To simulate the scour effect, a homemade double household shower device with an adjustable tap is used to control water flow. The test rainfall is determined according to the weighing method to determine. The principle is to place a round mouth fitting with a diameter of 20cm underneath the spraying device located 50cm above the fitting. The rainfall is measured by the simple conversion, where every 30g of water corresponds to 1mm of rainfall.



Figure 8. Double mounting device.

2.4. Testing program

According to the model box size, a 1:25 scale model slope M-1 with a height of 200mm was prepared, and a 5m high cutting slope of the coastal highway was simulated. The field sand sample with layered compaction (four layers) and sprinkling model was dried to control the moisture content at 20%. The slope gradient was set at 1:1. The basic parameters of the slope model are shown in Table 4. During the test, changes in pore pressure during the perfusion process and scouring action were measured by the embedded pore pressure sensor. The buried position of the sensor is illustrated in Figure 9. 1, 2 and 3 were vertically arranged along the depth direction, with a separation of 50mm. Sensors 2, 4 and 5 were located at the same horizontal line, 100mm below the top surface of the slope.

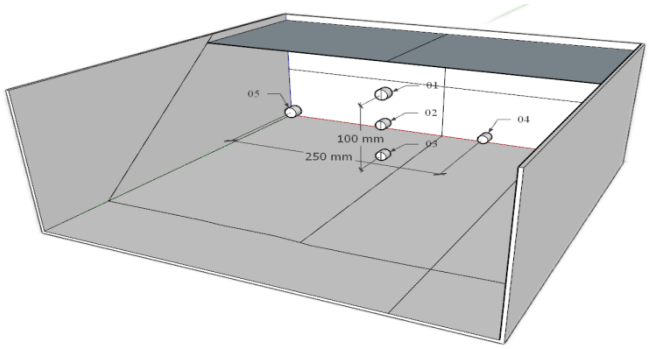


Figure 9. Internal sensor buried location diagram.

Table 4. M-1 Basic parameters of slope model.

Slope base length	Crest length	Slope height	Slope gradient	Moisture content	Reduced scale
300mm	100mm	200mm	1：1	20%	1:25

To facilitate the observation of displacement and deformation of the model under the action of scouring, displacement monitoring pushpins were arranged on the surface. These pushpins were spaced at 5cm intervals along the transverse and slope direction. At the top of the slope, a row of displacement monitoring pushpins was arranged, precisely located at the leading edge of the slope. Four rows were arranged on the slope to construct the thumbtack surface monitoring point system. Each thumbtack was inserted 5mm deep into the soil to ensure that the model sand sample was minimally disturbed, as shown in Figure 10.



(**a**) (**b**)

Figure 10. Experimental model display.

The cementing solution was selected with a mix ratio of 1:0.5 (CaCl2: urea). First, CaCl2 fixative solution with the same volume and concentration of 1M was injected before the injection of bacterial solution. The injection process consisted of three sets of rounds, where the primary fixed solution + primary bacterial solution + primary cementing solution were injected into the sprinkler irrigation device in the order of fixed solution - bacterial solution - cementing solution, as shown in Table 5 for their respective volumes. The M-1 model underwent reinforcement through sprinkler irrigation in three rounds. The overall model is shown in Figure 11.

Table 5. Solution irrigation scheme.

Stationary liquid	Bacteria solution	Consolidating fluid	Time interval between the three solutions
1000mL	1000mL	2000mL	10min

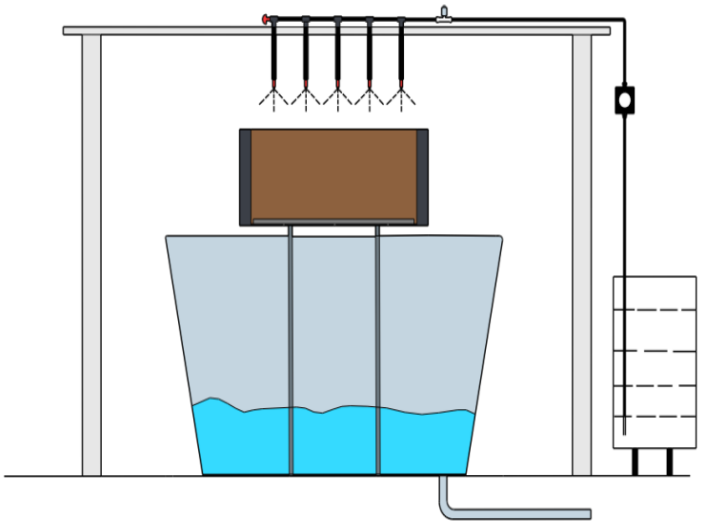


Figure 11. Overall model design.

Experimental analysis

3.1. Pore water pressure

The more loose particles in the model, the greater the bacterial adsorption capacity. The sand sample with a smaller particle size will affect the change of pore structure of the sand model, with a reduced permeability coefficient. During the continuous reinforcement process, the permeability coefficient k weakens due to a gradual reduction in the pores of the upper sand sample [19]. As bacillus liquid and fixed liquid flow through the sand sample model, pore water pressure in the pores will change with the seepage effect. In addition to surface runoff, a portion of the water flow direction in the sand sample also shows an infiltration effect [20][21]. After multiple rounds of reinforcement, the pores on the top surface, inclined surface and inside the sand sample model become filled and connected due to the formation of calcium carbonate particles. The pore water pressure sensor can be used to explore the changes in pore pressure during reinforcement and pore characteristics after multiple rounds of reinforcement. He Xiaoying, Li Dong et al. [22] equipped the laboratory with debris flow two-phase bodies to observe the change rule of pore water in debris flow sediment reinforced by MICP. They found that calcium carbonate generated by MICP solidification has a tendency to retain pore water pressure. In drainage consolidation tests, it was observed that when the sediment porosity was low, it was difficult to drain and consolidate. Li Xian proposed a theoretical formula for the grouting capacity of sand with different permeability coefficients of MICP, which provides a reference for whether the soil is suitable for reinforcement by the MICP method [23].

The pore water pressure test was divided into two stages. In the first stage, the M-1 model was injected with several different volumes of fixed liquid and bacterial liquid, and the change rule of the internal pore water pressure was measured by the embedded pore water pressure sensor inside the slope. In the second stage, a self-made rainfall de-

vice was used to simulate a certain rainfall intensity, and explore the change process of pore water pressure from initial moisture content to saturation point of the entire sandy slope until its internal water pressure law becomes unstable [24].

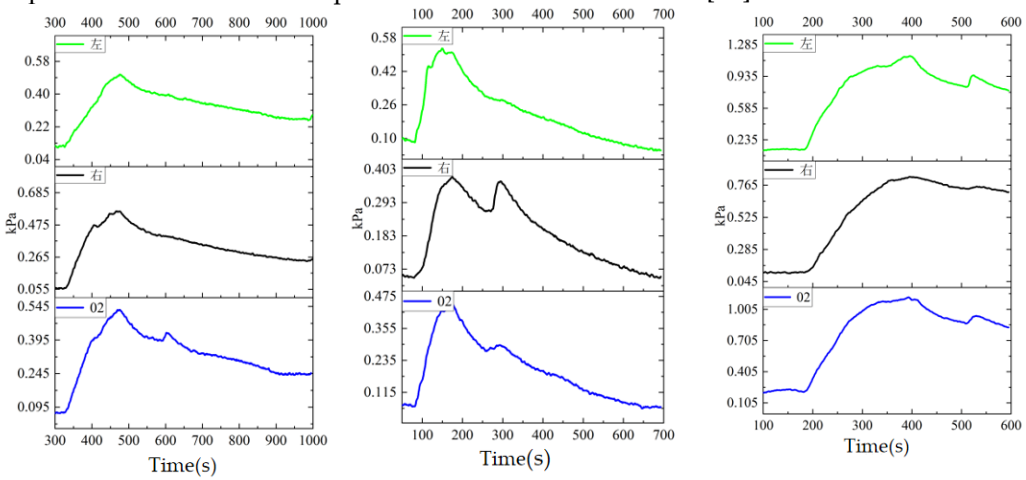
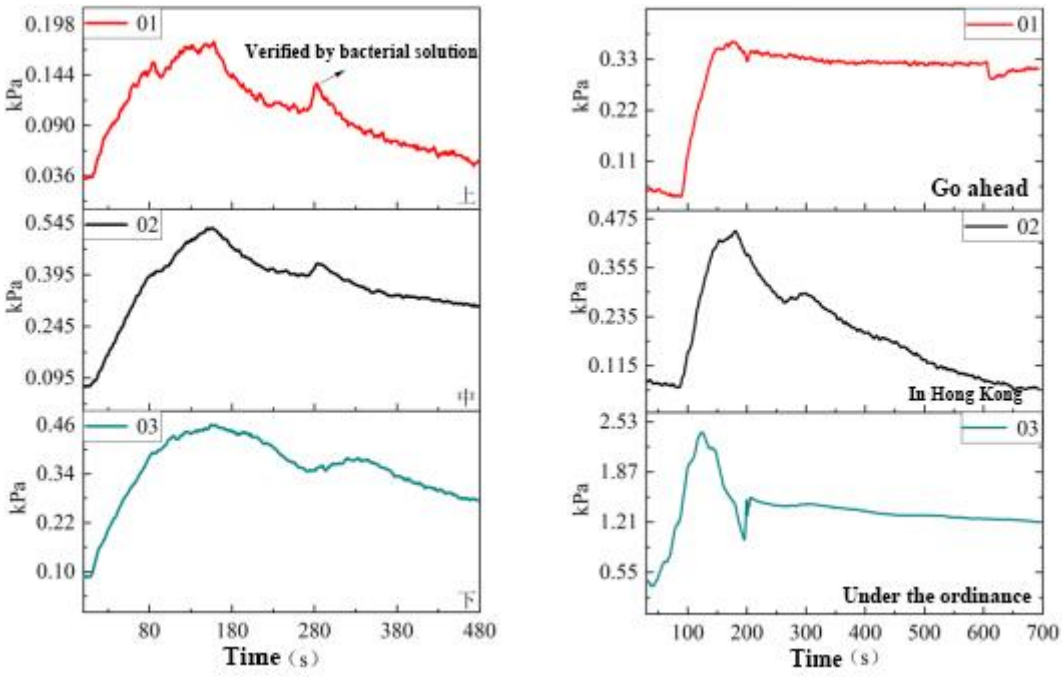


Figure 12. Horizontal direction of the first, second, third wheel reinforcement pore pressure changes.

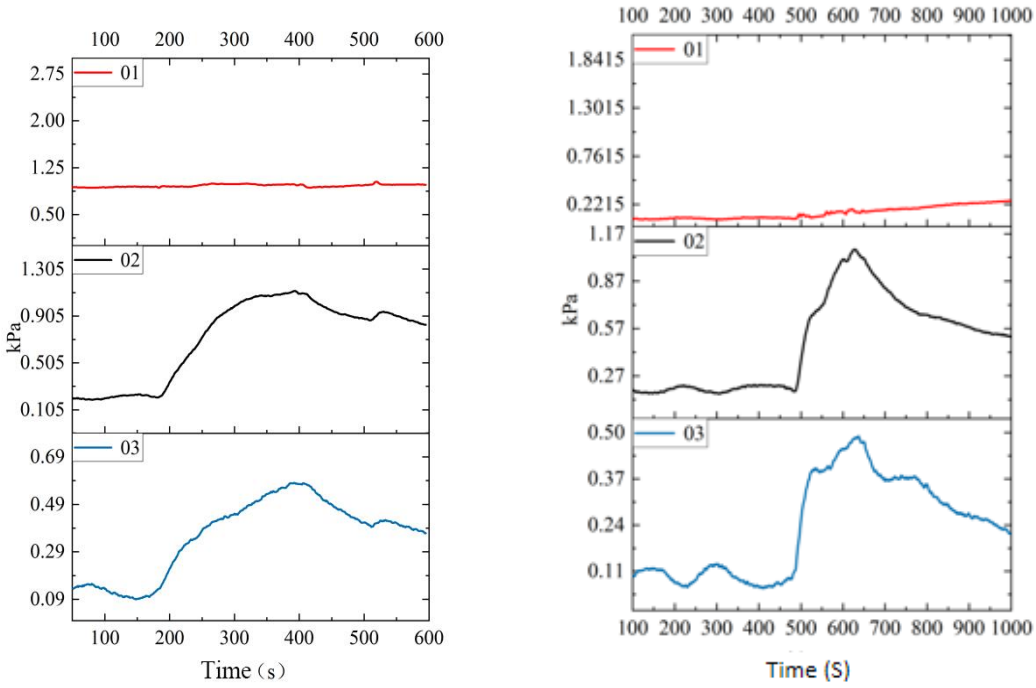
As observed from Figure 12 (a), the 02 sensor in the middle and the sensors on both sides of the same horizontal plane the solution infiltration channel was concentrated in the middle of the M-1 model during the first reinforcement, and the signals in the middle channel were very clear and distinct, while the signals at both ends of 02 were not as evident, and the pore pressure variation law was basically similar. Moving on to signal (b), during the second reinforcement, the seepage channel was concentrated on the right side of the model, and the secondary wave crest on the left side was not as pronounced. The variation of time-pore pressure in the horizontal direction of the third round of reinforcement (c) indicates that the seepage channel is located on the left of the center of the model. The test results show that after three rounds of perfusion reinforcement, the changes in pore pressure in the horizontal plane, specifically 10cm away from the top surface, exhibit clear sensitivity to the seepage layer. At this depth, the calcium carbonate products are comparatively lower, with ordinary filling effect, and the curing effect is not particularly noticeable at this depth.



(**a**) (**b**)

Figure 13. Pore pressure changes in the first and second rounds of cementing fluid.

From FIG. 13, it is evident that pore pressure undergoes changes from top to bottom during the cementing process. Sensors 02 and 03 show a certain time lag compared with 01, and the size effect is more obvious. First, to verify the possible interaction between the bacterial solution and the cementing solution on pore pressure changes, a test was conducted where 400mL bacterial solution was injected at 280s for 20s. The test results show that the rising rate of the shallow sensor 01 is the fastest after the mixing of cementing liquid and bacterial liquid, signifying an obvious reaction of calcium carbonate surface. However, after the rise of pore pressure at the bottom, the secondary wave crest changes minimally, and the pore pressure dissipates for an extended period. As a result, the pore pressure change rate of 01 at the secondary wave peak is not as high as that of 02 and 03 at the bottom. The results suggest that the reactants gradually reduced, and the formation of calcium carbonate was more obvious in the shallow reaction, hindering the infiltration of the solution. However, in Figure (b), after 01 began to rise, the pore pressure remained constant at 0.33kPa for about 500s. This indicates that, in the shallow depth range, due to the shallow reaction of calcium carbonate, after filling the sand pores, the pores slowly decrease until completely filled. In terms of pore pressure law, the change rate of pore pressure weakens and remains unchanged for a certain period, approximately forming a kind of "calcium carbonate film" that stablized pore pressure. However, sensors 02 and 03 below can still perceive the change of pore pressure after solution infiltration. Pore pressure rises quickly within a certain period, and the process of pore pressure dissipation also indicates a gradual decrease in pore water pressure in the model, reflecting the effect of infiltration. The accumulation of calcium carbonate in the surface pore of the model greatly affects the changes in surface pore pressure.



(**a**) (**b**)

Figure 14. Pore pressure changes in the third round of reinforcement when bacteria liquid and cementing liquid pass through.

FIG. 14 (a) and (b) respectively show the time-pore pressure variation of bacterial and cementing fluids in the third round of reinforcement. The continuous changes in pore pressure in this cycle reaffirm the plugging effect of calcium carbonate "film" formed in the middle pores of the upper part of the model. The previous stone of sensor 1 is blocked by the products near the measuring point of sensor 1, and the stabilization of calcium carbonate around the sensor results in a minimal pore pressure change rate, showing a straight line on the graph. On the other hand, the deep sensor is characterized by a dynamic equilibrium process from shallow to deep, indicating that the deep solidification is not significant and the lower pore cementation effect is poor. Pore water during grouting is represented as a dynamic infiltration process, on which the pore pressure changes of 01 in the three groups are mapped. As shown in FIG. 15, after three times of irrigation with bacterial and cementing fluids, the pore water pressure at 01 gradually decreases. Compared with the second irrigation, the decrease of the first irrigation is the most obvious, which can be attributed to the large amount of calcium carbonate generated in the first two irrigation, filling most of the voids and leading to a minor change in the graph between the third irrigation and the second irrigation. This suggests that the downward infiltration of bacterial and cementing fluids in the third irrigation was affected by the substantial amount of calcium carbonate generated in the previous two irrigations, confirming the conclusion that the deep curing effect was not significant.

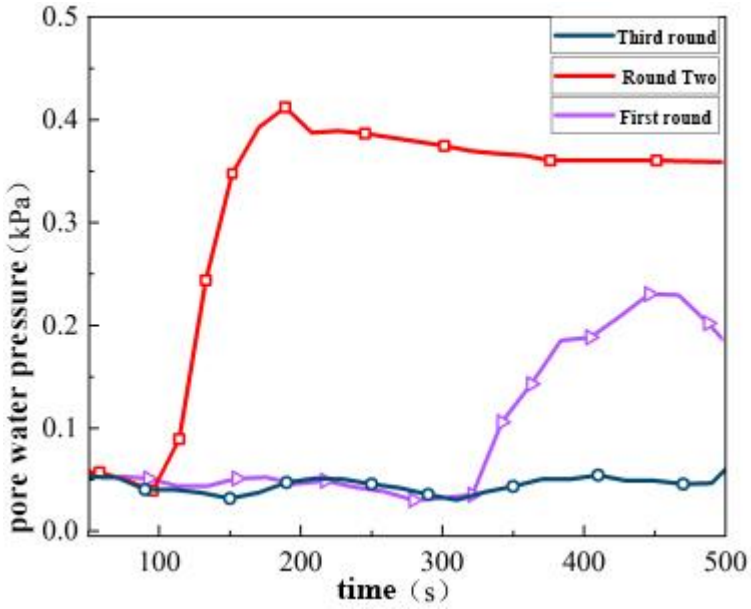


Figure 15. Changes of 01 time - pore pressure in three rounds

By idealizing the slope model, the failure of the model can be divided into three stages under the short-duration and high-intensity rainfall condition. The overall time-pore pressure variation diagram for 01-05 sensor and the time-pore pressure variation diagram for different time periods are shown in the figure below.

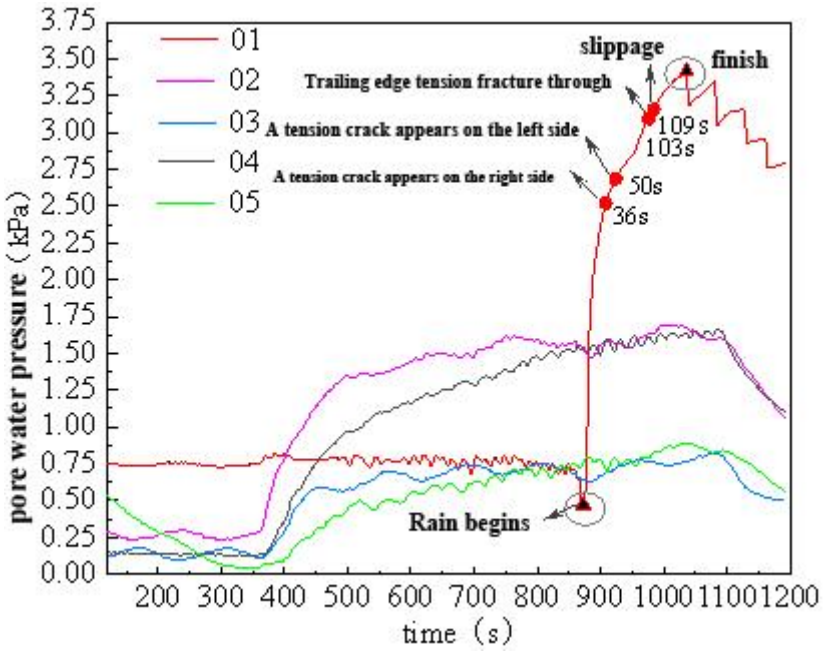


Figure 16. Variation of 01-05 pore pressure during rainfall.

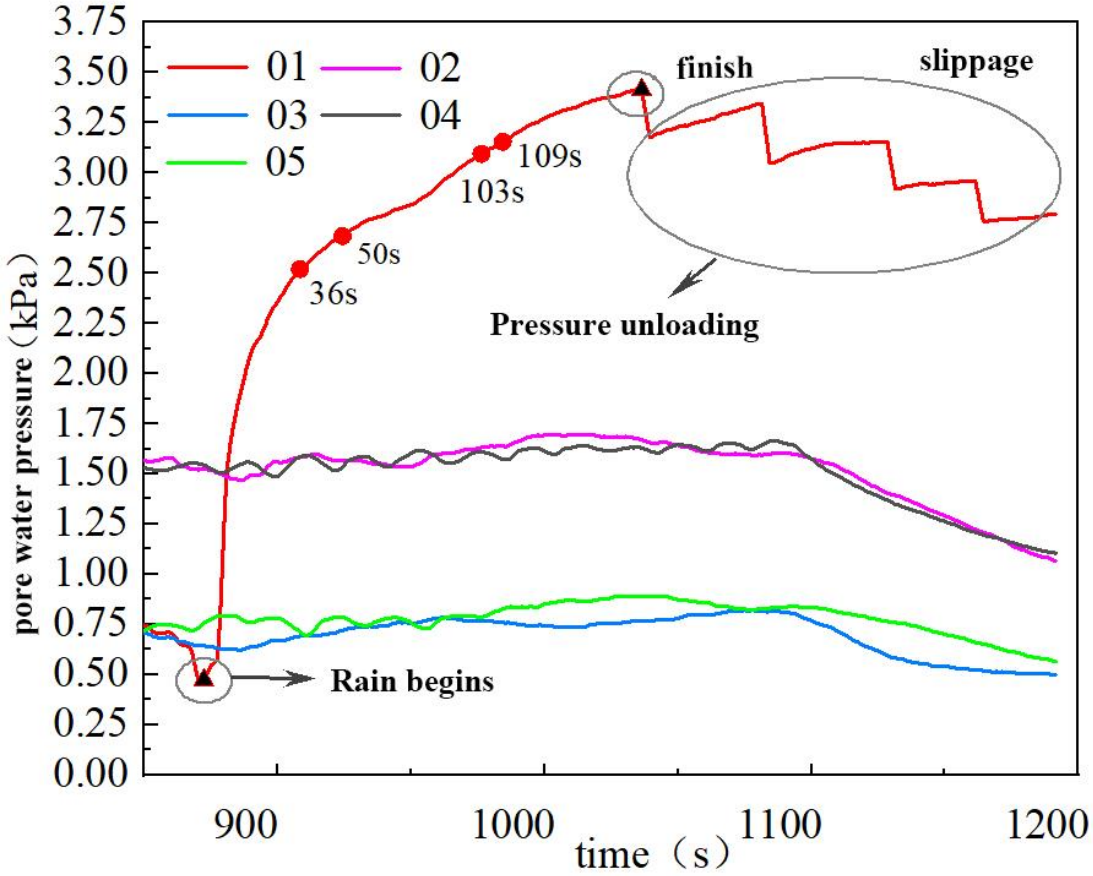


Figure 17. 01-05 Sensor rainfall duration-pore pressure change from 850-1200s.

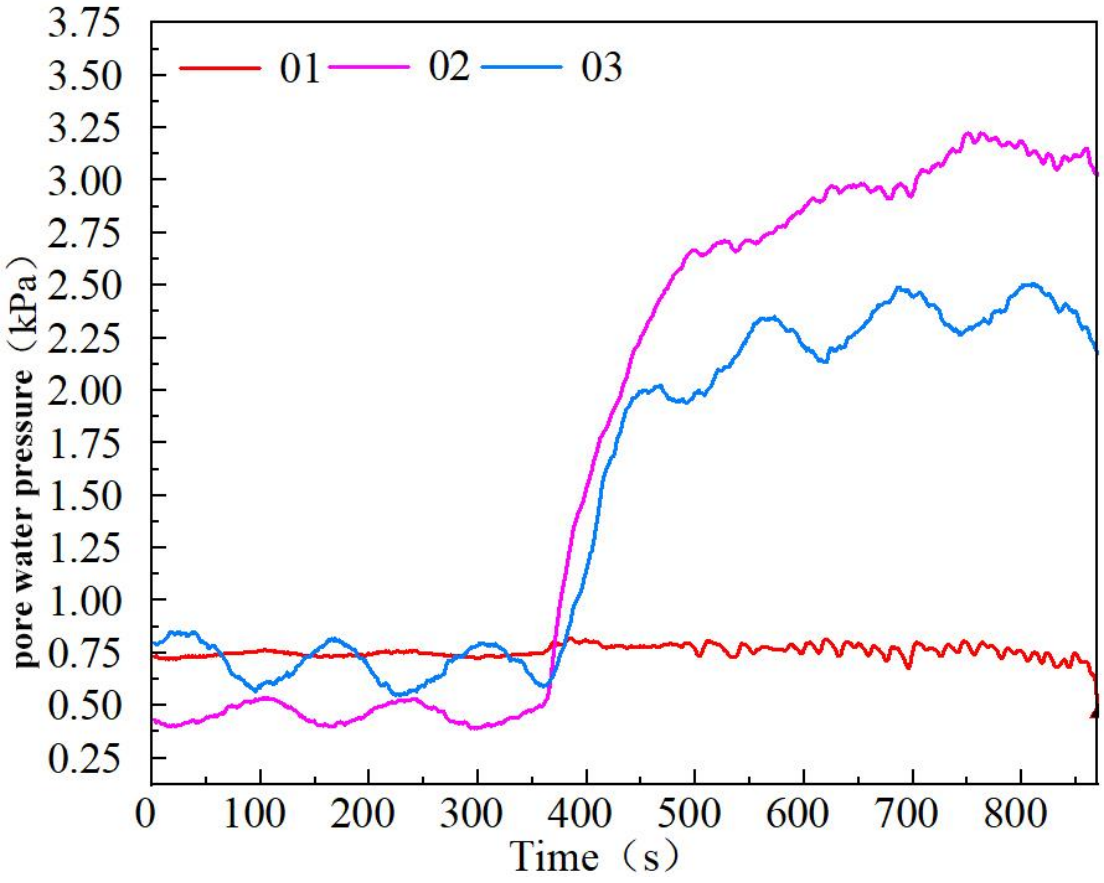


Figure 18. 01-03Pore pressure changes when the sensor is 0-800s.

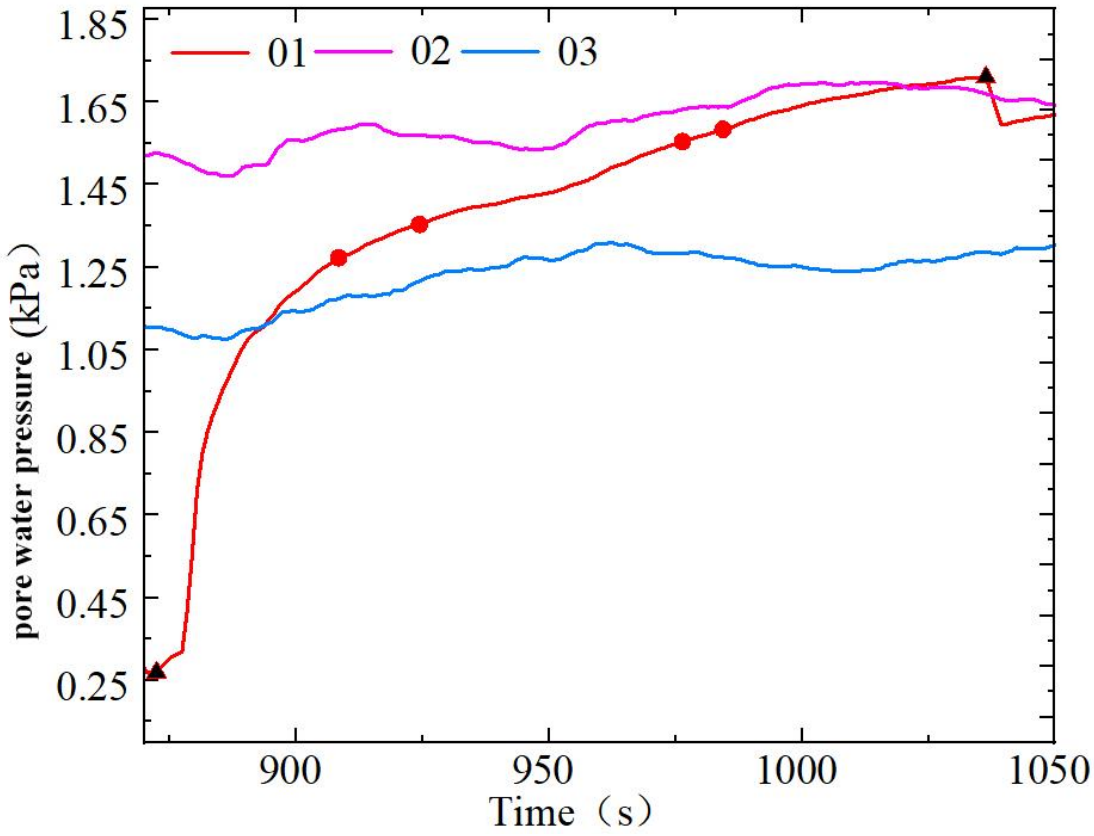


Figure 19. 01-03 Sensor pore pressure change from 800 to 1050s.

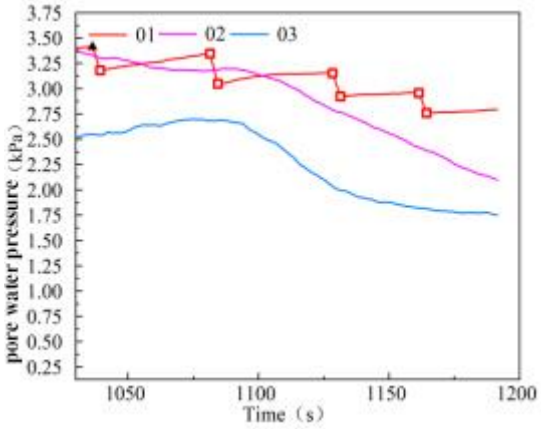


Figure 20. 01-03Pore pressure change of the sensor at 1050-1200s.

According to the analysis of FIG. 16,17,18,19 and 20, the first stage is the infiltration stage. Based on the pore pressure changes in this stage, the pore pressure change rate of 01 is close to zero due to the existence of a calcium carbonate "diaphragm" in the pores of the sand body, as characterized by sensor 1. Solution percolation exists in the M-1 model. When pore pressure drops in No. 02 of the upper part, the solution percolates downward, while pore pressure rises in No. 03, exhibiting a top-down seepage change feature. The second stage is the rainfall stage. From 872s, due to the surface solidification, the cementation of the slope surface and the top area is obvious. The rainfall is mostly transformed into runoff flowing down the slope surface, and the slope surface enters a transient saturation state. However, the cementation of calcium carbonate on the surface limited the infiltration of a large amount of water, and the pore pressure of 02 and 03 did not change significantly. Due to the increase in water content, the decrease in basement suction leads to a decline in slope stability. When the slope begins to slip at 109s, the basement suction in the soil becomes zero, and the slope model starts to slide and fail. After 160s, the rainfall ends. The third stage is the sliding unloading stage, starting from 1033s. After the rainfall, the overlying pressure continues to unload, the slope is damaged in stages, causing the pore pressure to decrease in a stepped way. The pore pressure deformation law of the slope without MICP reinforcement should be a broken line of slow decline after failure. However, after MICP reinforcement, the creep of the S-3 slope is very slow after the rainfall stopped. Due to the cementation in the sand body, the pore pressure in the slope discharges in a stepped manner, and the basement suction undergoes a process of repeated rise and then decline. After MICP reinforcement, the slope can maintain certain stability after failure and prolong the creep time.

3.1. Fluid-slip pattern

After three rounds of reinforcement on the slope of M-1 model, a simulation of short-duration high-intensity scour action was conducted, and the flow rate of the scour device was measured. According to the regulations of the national meteorological department, the rainfall of 23mm reached the heavy rain level within 12 hours (15mm-29.9mm), and the rainfall intensity was 23mm/min, exceeding the local average daily rainfall standard in Dongfang City. The damage morphology of M-1 was observed after being scoured.

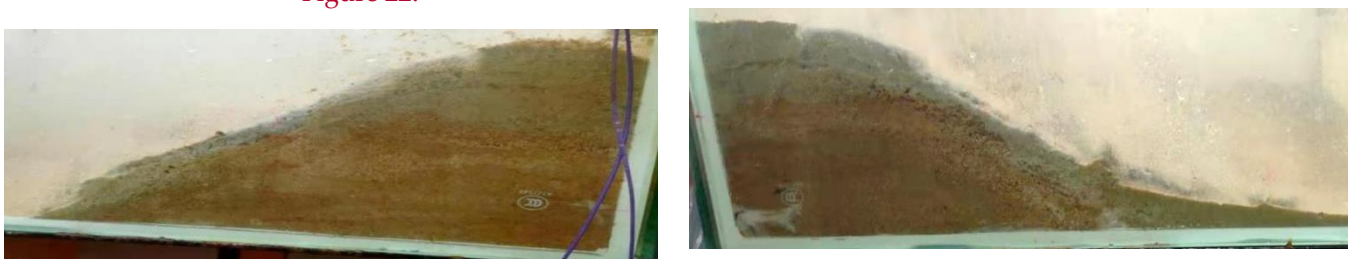
At 150s, M-1 failed under the rainfall simulation, and the slope experienced a prolonged period from the beginning of erosion to sliding failure. After the erosion of rainfall intensity, the failure mode manifested as the overall sliding failure of the slope. After 36s, the fracture began to develop on the right side of the M-1 slope top, with a diagonal fracture length of 4cm and a width of 2mm. After 50s, the left oblique crack started to develop, measuring 6cm in length and 2mm in width. The sand on the slope surface remained intact despite the entrainment runoff, making it resistant to loss. Approximately

103s into the process, the oblique cracks on both sides connected, and the tension cracks appeared at the rear edge of the slope top, with a width of the cracks of 3mm. These cracks were distributed in a circular arc. The green thumbtack band on the slope top moved downwards. The left side of the slope surface was missing, and the red pushpin belt at the slope angle began to deform. The slope foot experienced unloading. The moisture content of the lower soil was close to saturation, but the slope body integrity was well-maintained. Refer to Figure 21 for further details.



Figure 21. Integral slip.

At 115s, the scour effect leads to an increase in the internal water content of the soil, causing a decrease in effective stress and the anti-sliding force of the soil. Consequently, the slope surface of the model begins to slide downward as a whole. The development of tension cracks induces rainfall convergence, and the infiltration of rainwater further raises the water content of the model, which accelerates the sliding of the slope. Despite some surface damage, the model maintains good overall integrity. The failure characteristics of the model are different from those of the model without MICP reinforcement. The sliding surface inside the slope can be seen from the lower M-1 side view, and it can be inferred that the sliding surface is located at 4-5cm depth. For further details, refer to Figure 22.



(**a**) (**b**)

Figure 22. M-1 Model slippage side view.

When the simulated rainfall effect was stopped, the slope model morphology was divided from the front and top surfaces due to the development of cracks. The surface sand of the slope block remained intact, and the segmented blocks had a thickness of about 3-4cm. After 150s of simulated scour, the model experienced damage. The failure characteristics of MICP solidified slope model M-1 are manifested as fractional sliding. Due to sand loss, the front edge of the model exhibits an unloading effect and the largest deformation. After slope angle slip and accumulation, the upper slope continues to slide and deform slowly. The damage integrity of the model after MICP action remains good

in the short-duration and high-intensity simulation of rainfall, and MICP spray irrigation curing technology can effectively resist surface erosion. For further details, refer to Figure 23.



(**a**) (**b**)

Figure 23. Front and top slope.

4. Conclusions

(1) In the M-1 model, after two rounds of reinforcement, a calcium carbonate "film" was formed in the shallow pores of the slope, which reduced the pore pressure change rate during the infiltration of the solution. The model first reacts to produce calcium carbonate in the shallow layer, leading to a solidification of the shallow layer and a gradual decrease in the space between sand particles. The lower part of the model demonstrates the process of solution infiltration, and the secondary wave crest rises slowly, indicating that the product prevents solution infiltration. The pore pressure of the sensor at the same horizontal depth follows the same change law. However, below 10cm of the top surface, there are fewer products, with a larger pore pressure change rate and general curing effect.

(2) The S-3 slope, strengthened by three sets of turns, failed after 150s. The surface blocks of the slope were divided due to the development of cracks. The thickness of the divided blocks was about 3-4cm. After 109s of rainfall, the moisture content of the soil increased, with a decrease in effective stress and anti-sliding force of the soil and the slope surface of the model as a whole. The development of tension cracks induces rainfall convergence and accelerates slope slip. Despite some surface damage, the model maintained good overall integrity. The failure characteristics of the slope are manifested as fractional sliding. Due to the loss of sand, the unloading effect of the model front is obvious, and the deformation is the largest. At the onset of the slip, the suction of the base became zero, and the failure form shows an overall slip with subsequent creep unloading.

(3) After MICP reinforcement, the creep of the M-1 slope model is very slow. The cementation in the sand body leads to the discharge of pore pressure in the slope in a stepped manner, and basement suction undergoes a process of rising and then falling repeatedly. MICP slope can maintain a certain integrity after failure, prolong the creep time, improve the water stability and anti-erosion capacity of MICP slope under the action of heavy rainfall, and enhances the safety factor of the slope.

Author Contributions: Conceptualization, J.N. and Y.P.; methodology, M.J.; software, Z.K.; validation, J.C.; formal analysis, M.J.; investigation, W.H.; resources, Z.K.; data curation, J.C.; writing—original draft preparation, Y.L.; writing—review and editing, Y.P.; visualization, M.J.; supervision, Y.L.; project administration, J.N.; funding acquisition, Y.L. All authors have read and agreed to the published version of the manuscript

Funding: Please add: This research was funded by the Research and application of intelligent construction technology and intelligent management of ky Marine Building（ZDKJ2021024）, the Study on microbiological reinforcement technology of silty sand Subgrade in coastal area(521RC1040) and Study on high performance supporting structure of coastal tunnel with high water pressure(522CXTD510).

Institutional Review Board Statement: Not applicable

Informed Consent Statement: Not applicable

Data Availability Statement: Not applicable

Conflicts of Interest: The authors declare no conflict of interest.

References

1. He Jia, Chu Jian, Liu Hanlong, Gao Yufeng, Li Bing. Research progress of microbial geotechnical technology [J]. Chinese Journal of Geotechnical Engineering,2016,38(04):643-653.
2. DEJONG J T, FRITZGES M B, NÜSSLEIN K. Microbially induced cementation to control sand response to undrained shear[J]. Journal of Geotechnical and Geoenvironmental Engineering, 2006, 132(11): 1381－ 1392.
3. Al Qabany A, Soga K. Effect of chemical treatment used in MICP on engineering properties of cemented soils. Géotechnique, 2013, 63(4): 331-339.
4. Guanghui Shao, Haitao Chen, Min Hou, Rongpin Huang, Peng Liu. Variation characteristics of mineralization reaction of silty soil solidified by microbial grouting [J/OL]. Chinese Journal of Geotechnical Engineering :1-7[2022-06-22].
5. Li Xian, Wang Shixiang, He Binghui, Shen Taiyu. Soil and Rock Mechanics,2019,40(08):2956-2964+2974.
6. Xu Pengxu, Wen Zhili, Yang Simeng, Liu Zhiming, Leng Meng, Peng Jie. Experimental study of MICP-solidified sand under different particle sizes [J]. Geological Journal of China Universities,2021,27(06):738-745.
7. Whiffin V S.Microbial CaCO3 precipitation for the production of biocement[D].Perth Australia: Murdoch University, 2004.
8. Ma Ruinan, Guo Hongxian, Cheng Xiaohui, Liu Jingru. Experimental study on permeability characteristics of reinforced calcareous sand by microbial mixing [J]. Rock and Soil Mechanics,2018,39(S2):217-223.
9. LIU L, LIU H, STUEDLEIN A W, et al. Strength, stiffness,and microstructure characteristics of biocemented calcareous sand[J]. Can Geotech J, 2019, 56(10): 1502–1513.
10. Fang Xiangwei, Li Jingxin, Li Jie, Shen Chunni. Triaxial compression test and damage constitutive model of microbial solidified coral sand [J]. Rock and Soil Mechanics,2018,39(S1):1-8. (in China)
11. FENG K, MONTOYA B M. Influence of confinement and cementation level on the behavior of microbial-induced calcite precipitated sands under monotonic drained loading[J].Journal of Geotechnical and Geoenvironmental Engineering,2016, 142(1): 04015057.
12. Yi Manbing, Wang Yanning, Liu Dong,Ankit Garg, Lin Peng. Experimental study on coastal soft soil reinforcement based on microbial induced calcium carbonate precipitation technology [J]. Journal of Shantou University (Natural Science Edition),20,35(03):47-54.
13. Tang Yang. Study on solidification characteristics and fracture mechanism of microbial cemented sand body [D]. Tianjin University,2018.
14. Yin Liyang, Tang Chaosheng, Xie John, Lv Chao, Jiang Ningjun, Shi Bin. Effects of microbial mineralization on properties of rock and soil materials [J]. Rock and Soil Mechanics,2019,40(07):2525-2546. (in Chinese)
15. Hu Mingjian, Wang Nyum, Zhang Pingcang. Experimental study on slope stability and induced landslide under Rainfall condition: A case study of landslide piled breccia soil slope in Jiangjiagou Basin [J]. Chinese Journal of Geotechnical Engineering,2001(04):454-457.
16. Hu Qizhi, Liu Tongde, Ding Zhigang, et al. Effect of rainfall infiltration on stability of slope reinforced by microbial grouting [J]. Southern Agricultural Machinery,2021,52(08):5-8+14.
17. Wang Zhaoyang, Wang Jungang, Xu Renyu, Yao Xin, Li Yifan. Pore pressure characteristics of sand caused by water level rise and fall [J]. Journal of Shandong University of Technology (Natural Science Edition),2022,36(02):77-80.
18. Zeng Qiang, Influence of unsaturated seepage characteristics on slope stability [J]. Water Resources Science and Cold Area Engineering,2022,5(01):10-14.
19. Yuan Xiaolu, Zhou Shihua. Research on Application of MICP in Building Materials [J]. Yangtze River,2012,43(03):76-79.
20. Xu Pengxu, Wen Zhili, Yang Simeng, et al. Experimental study of MICP-solidified sand under different particle sizes [J]. Geological Journal of China Universities,2021,27(06):738-745.
21. Zhou Yi-zheng, Guan Dawei, Cheng Liang. Application of microbial induced carbonate in soil reinforcement [J]. Geological Journal of China Universities, 201,27(06):697-706.

22. He Xiaoying, Li Dong, Ren Yongbiao, et al. Study on the effect of MICP on the consolidation characteristics of viscous debris flow sediments [J]. Yangtze River,2021,52(06):148-153.
23. Li Xian, Wang Shixiang, He Binghui, et al. Soil and Rock Mechanics,2019,40(08):2956-2964+2974.
24. Tang Zhaoguang, Wang Yongzhi, Duan Xuefeng, et al. Development and performance evaluation of micro-porous water pressure sensor with high frequency response [J]. Chinese Journal of Rock and Soil Engineering,2021,43(07):1210-1219+1375-1376.

Disclaimer/Publisher's Note: The statements, opinions and data contained in all publications are solely those of the individual author(s) and contributor(s) and not of MDPI and/or the editor(s). MDPI and/or the editor(s) disclaim responsibility for any injury to people or property resulting from any ideas, methods, instructions or products referred to in the content.